Joint Beamwidth and Number of Concurrent Beams Estimation in Downlink mmWave Communications

Joint Beamwidth and Number of Concurrent Beams Estimation in Downlink mmWave Communications

Nancy Varshney and Swades De
Department of Electrical Engineering and Bharti School of Telecommunication
Indian Institute of Technology Delhi, New Delhi 110016, India

***Abstract*—This paper proposes a sectored-cell framework for mmWave communication. It consists of multiple concurrent beams generated from a partially-connected hybrid precoder at an eNodeB (eNB) to serve a dense user population in urban scenarios. Multiple beams sweep the cell in a round-robin fashion to serve the sectors with fair scheduling opportunities. Each beam serves all the users located within a sector using orthogonal frequency division multiple access. We aim to estimate an optimum beamwidth and an optimum number of beams required to maximize the average of long-run user rates with a given power budget for transmission and hardware consumption at the eNB. Simulation results demonstrate that employing higher beams increases the side-lobe interference still, the achievable average long-run user rate improves on account of longer sector sojourn time and higher frequency reuse. On the other hand, employing a very narrow beam is also not optimal.**

***Index Terms*—mmWave communications, beamforming, concurrent beams, interference, optimal beamwidth, scheduling**

I. Introduction

For fifth and higher generation wireless networks millimeter-wave (mmWave) frequencies offer increased spectrum availability to meet the anticipated high data demands. In mmWave wireless communication, antenna beamforming is deployed to overcome high attenuation losses. A large number of antenna elements result in a narrow beam pattern of high directivity and reduced beam footprint. Therefore, hybrid beamforming has been proposed in the literature to enable concurrent transmissions using highly directed beams.

Hybrid transceiver structure divides the processing between analog beamforming at radio frequency (RF) level and digital beamforming at baseband level to reduce the required number of RF chains N_{RF}. It allows spatial time division multiple access in which each user (UE) gets a dedicated link of the data stream with an improved signal-to-noise ratio. Hybrid beamforming structure is of two types. One is a fully connected structure in which each antenna array element is connected to all the RF units and the other is the partially connected (or sub-array) structure in which each RF unit is connected only to a subset of antenna array elements. To exploit the benefits of narrow beams in achieving maximum throughput over every link and for the network, usage of massive MIMO is envisioned at mmWaves [1]. However, a large number of concurrent beams in massive MIMO is associated with high power consumption and signaling and computational overheads [2]. A majority of work at mmWave communications have extensively investigated various hybrid beamforming designs for narrowband and wideband mmWave channel for single as well as multi-user scenario.

A. Related work and motivation

In the fully-connected hybrid beamforming structure, the joint estimation of optimal baseband and optimal RF precoding matrix to maximize spectral efficiency and reduce inter-beam interference is a Non-deterministic Polynomial-time (NP)-hard optimization problem [3]. Also, the precoding complexity grows exponentially with increasing UE density. Nevertheless, sub-array hybrid beamforming is a competent design at mmWaves communication [4]. However, the high power consumption associated per RF chain is a major limitation in the deployment of such systems to serve high UE population with a dedicated link to each in the urban micro (UMi) environment.

The work in [5] proposed to allocate the wideband channel to the same UE by considering a high correlation among subcahnnels leveraging sparsity of mmWave channel. However, the authors did not consider the beam-squint factor of large antenna arrays into the analysis [6]. Nonetheless, the mmWave channels show frequency-selective nature because of the huge bandwidth range (on the order of giga-Hertz) as well as the mobile environment. In [7], frequency-selective mmWave wideband channel was proposed to be used such that N_{RF} RF units jointly serve U UEs per subchannel, requiring $N_{RF} \geq U$. For sub-array design, in [8] the authors proposed cross-entropy optimization for optimal analog precoder search. A hybrid precoding design was proposed in [5] to maximize the downlink sum-rate under a subcarrier power constraint. This approach does not sufficiently exploit the spatial degree of freedom resulting from narrow beamwidth. The authors in [9] suggested iterative phase updates of RF precoder to minimize the squared error between optimal full-baseband and the hybrid design. All these works considered UE density, M, in a wideband mmWave scenario such that $M \leq N_{RF}$, and the fact that each beam serves only one UE over the wideband channel. However, the allocation of the whole mmWave bandwidth to a single UE is not an optimal strategy. Hence, due attention is required to utilize this frequency-selective nature of mmWave channels for designing optimal mmWave communications systems for a high-density multi-user environment.

An increasing number of concurrent beams in a cell will induce more interference at a UE. A RF precoder was designed

in [10] using block diagonalization to cancel the inter-user interference. However, the maximum number of null directions is limited by the available number of RF chains at the baseband precoding stage, thereby setting a constraint on the maximum number of scheduled UEs in an epoch. The work in [11] suggested increasing transmit beamforming gain to overcome inter-user interference. But, there is a limit on the maximum radiation intensity. Hence, increasing the transmit beamforming gain without any constraint is not practical. Further, for high UE density scenario, i.e., $U \gg N_{RF}$, UE grouping methods were proposed in [12] and [13] that used channel correlation and angle-of-departure (AoD) of the UEs, respectively, to group them at the RF precoding stage. After that, the data to the UEs is transmitted over the dominant channel eigenmodes to reduce inter-user interference. Again, these works assume a dedicated beam per UE at time.

To this end, we observe dedicating an RF unit along with the entire spectrum to a single UE at a time in a UMi environment is not advantageous from the spectral and energy efficiency perspective. The preliminary work in [14] investigated the optimum transmit beamwidth required to maximize system performance when an eNB has a single RF chain. Therefore, the analysis was devoid of inter-beam interference. As an extension, in this paper, we analyse the behaviour of the sectored-cell model employing multiple RF chains at the eNB while incorporating the resulting inter-beam interference analysis. To the best of our knowledge, the proposed system model has not been studied in the literature yet.

B. Contribution

The key contributions are:

1. A novel system model is presented to serve multiple UEs in the UMi scenario utilizing the frequency-selective property of the mmWave channel using sub-array hybrid beamforming design.
2. A optimization problem is formulated to jointly estimate the optimum number of sectors and the optimum number of concurrent beams that achieves maximum average long-run UE rate for a given eNB power budget.
3. Also, a comparison of scheduling complexity of the sectored-cell framework over the existing competitive scheduling hybrid beamforming designs in the literature is provided.

The advantages of using the proposed approach are:

(a) Codebook size contains only the weight vectors of phase-shifters corresponding to fixed and limited steering directions. This mitigates the problem of finding optimal phase-shifter weights in hybrid precoding.
(b) Beam in each sector is able to serve multiple UEs in an epoch. All UEs that are able to sense the beam in a sector connect to the eNB. Hence, the computationally complex eNB-UE beam pair search is not needed.
(c) Scheduling of UEs is computationally less complex.

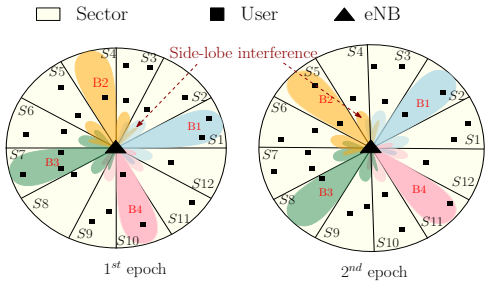

Fig. 1. Pictorial representation of round-robin scheduling of sectors in a cell with $S = 12$ sectors represented as $\{S1, \ldots, S12\}$ and $N_{RF} = 4$ beams represented as $\{B1, B2, B3, B4\}$.

II. System Model

We consider a small cell downlink mmWave system in UMi environment. Let U be the number of single antenna UEs uniformly distributed in the cell. We partition the cell into S similar sectors. Let $\mathcal{S}$ be the set containing all possible values of S that a cell can be sectorized into, i.e., $\mathcal{S} = \{S | S = \lceil \frac{2\pi}{\theta} \rceil, \theta_{min} \leq \theta \leq \theta_{max}\}$. Here, θ_{min} and θ_{max} are, respectively, the minimum and the maximum sector beamwidth equivalent to half power beamwidth (HPBW) of a beam formed with a uniform linear array (ULA). Let s and $K(s)$ denote the index of a sector, i.e., $s = \{1, 2, \ldots, S\}$ and number of UEs located in s^{th} sector such that $\bigcup_{s \in S} K(s) = U$, respectively, given a particular sectorization scheme $S \in \mathcal{S}$.

At eNB beamforming is employed with N_{RF} RF chains, placed to cover entire 2π radians, that concurrently serve UEs located in N_{RF} out of S sectors in an epoch. We consider that each RF unit is connected to a separate ULA (or a sub-array) consisting of N_t antenna elements constituting a beam. In an epoch of duration T, each beam serves all the UEs in the corresponding sector using OFDM. The N_{RF} concurrent beams serve the sectors in a fashion such that during t^{th} epoch all the beams are distributed uniformly apart over 2π radians. During the $(t+1)^{th}$ epoch, all the concurrent beams switch in either clockwise or anti-clockwise direction simultaneously to serve the adjacent sectors. A schematic diagram of the proposed model with 4 beams in 12 sectors employing round-robin scheduling is shown in Fig. 1.

A. Wideband mmWave channel model

At mmWave the eNB-UE link is either line-of-sight (LOS) or non-line-of-sight (NLOS). The probability of k^{th} UE located at a distance d_k being in LOS is given as [15]

$$\Pr(d_k) = \min(D_1/d_k, 1)(1 - e^{-d_k/D_2}) + e^{-d_k/D_2} \quad (1)$$

where $D_1 = 18$ and $D_2 = 36$. Also, the path loss for LOS and NLOS link are given as [16]

$$\begin{aligned} \text{PL}_{LOS}(d_k) &= 61.4 + 20\log_{10}(d_k) + \mathcal{N}(0, 33.64) \text{ [dB]} \\ \text{PL}_{NLOS}(d_k) &= 72.0 + 29.2\log_{10}(d_k) + \mathcal{N}(0, 75.69) \text{ [dB]}. \end{aligned} \quad (2)$$

Consequently, for the k^{th} UE located at a distance d_k from the eNB the pathloss γ_k is given as

$$\gamma_k = \begin{cases} \Pr(d_k) 10^{\text{PL}_{LOS}(d_k)/10}, & \text{LOS} \\ (1 - \Pr(d_k)) 10^{\text{PL}_{NLOS}(d_k)/10}, & \text{NLOS}. \end{cases} \quad (3)$$

Since mmWave channel is a wideband channel it exhibits frequency-selective fading. So, we divide the total available bandwidth B is divided into N_c subchannels denoted as $\mathcal{N}_c = \{1, 2, \ldots, N_c\}$. Further, due to spares nature of mmWave the channel has $L_k \ll N_t$ multipath components (MPCs) [17]. Therefore, the channel coefficient between the eNB and k^{th} UE over n^{th} subchannel in s^{th} sector is given as

$$\mathbf{h}^s_{k,n} = \sqrt{\frac{N_t}{L_k \gamma_k}} \sum_{l=1}^{L_k} \alpha_{k,n,l} \mathbf{a}(\omega(f_n), \phi_{k,l})^H \in \mathbb{C}^{1\times N_t} \quad (4)$$

where $\alpha_{k,n,l}$ is small scale fading gain of l^{th} MPC over n^{th} subchannel, and $\phi_{k,l}$ is the AoD of l^{th} MPC. The array response vector $\mathbf{a}(\omega(f_n), \phi_{k,l})$ of the eNB at an offset angle $\phi_{k,l}$ is given as

$$\mathbf{a}(\omega(f), \phi_{k,l}) = \frac{1}{\sqrt{N_t}} \Big[1, e^{-j\frac{2\pi}{\lambda_c} d' \omega(f) \sin\phi_{k,l}} \ldots, e^{-j\frac{2\pi}{\lambda_c} d' \omega(f)(N_t-1)\sin\phi_{k,l}}\Big]^T. \quad (5)$$

The factor $\omega(f) = (1 + f/f_c)$ is the beam squint parameter at frequency f [6], f_c is the carrier frequency, d' is the inter element ULA spacing, and λ_c is the carrier wavelength. We assume that the information of $(L_k, \alpha_{k,l}, \phi_{k,l}, d_k)\ \forall k$ is available at the eNB.

The maximum gain of ULA is given as $G = N_t \bar{g}$, where $\bar{g}$ is the single antenna element gain. Correspondingly, the HPBW of the beam is $\approx 2/N_t$ [18]. Further, we set the value of the effective isotropic radiated power (EIRP) high enough to overcome high attenuation as well as low enough to be below the maximum EIRP level allowed by Federal Communications Commission (FCC) specifications [19]. Fixing the EIRP, by appropriate power control, we also ensure that the beam coverage range is static regardless of width of the beam. Let P_{total} be the total transmit power required by an RF chain to generate a beam of θ_{max} HPBW given an EIRP value. Then, for a beamwidth $\theta < \theta_{max}$ the transmit power required to guarantee same radiated power density at distance d is calculated as

$$P_T = \frac{\text{EIRP}}{G_\theta} = \frac{P_{totat} G_{\theta_{max}}}{G_\theta} = \frac{P_{total} N_t(\theta_{max})}{N_t(\theta)} \approx \frac{P_{total}\theta}{\theta_{max}} \quad (6)$$

where $G_{\theta_{max}}$ and G_θ are the maximum ULA gain corresponding to HPBW θ_{max} and θ, respectively, and $N_t(\theta_{max})$ and $N_t(\theta)$ are the active number of elements in ULA corresponding to HPBW θ_{max} and θ, respectively.

B. Effective rate in presence of side-lobe interference

As the practical beam radiation pattern has side-lobes, a UE located in s^{th} sector served by b^{th} beam during an epoch will observe side-lobe interference from the rest of the concurrently active beams $\hat{b} \neq b$. Moreover, the wideband antenna array beamforming vector of a beam at eNB, steered at angle Φ_b, is given as:

$$\mathbf{A}(\Phi_b) = \frac{1}{\sqrt{N_t}} \Big[1, e^{-j\frac{2\pi}{\lambda_c} d' \sin\Phi^b} \ldots, e^{-j\frac{2\pi}{\lambda_c} d'(N_t-1)\sin\Phi^b}\Big]^T \quad (7)$$

In a sectorized cell, each beam serves S/N_{RF} sectors and the possible steering directions are fixed at $\Phi_b = (b-1)(360^o/N_{RF}) + (t-1)(360^o/S)$, where $t = 1, \ldots, \lceil S/N_{RF} \rceil$ denotes the epoch. Therefore, the signal-to-interference-plus-noise ratio $\Gamma^s_{k,n}$ of k^{th} UE at distance d_k from eNB, over n^{th} subchannel in sector s served by b^{th} beam is

$$\Gamma^s_{k,n} = \frac{P^s_{k,n} |\mathbf{h}^s_{k,n} \mathbf{A}(\Phi_b) \mathbf{A}(\Phi_b)^H {\mathbf{h}^s_{k,n}}^H|}{N_0 B/N_c + \sum_{j\in\mathcal{S}_i, j\neq s} P^j_{k,n} |\mathbf{h}^j_{k,n} \mathbf{A}(\Phi_j) \mathbf{A}(\Phi_j)^H \mathbf{h}^{jH}_{k,n}|} \quad (8)$$

where $\mathcal{S}_i \subset S$ is the set of sectors concurrently served by N_{RF} beams, $P^j_{k,n}(P^s_{k,n})$ and $\mathbf{h}^j_{k,n}(\mathbf{h}^s_{k,n})$ are the power allocation and channel vector of k^{th} UE over n^{th} subchannel in $j^{th}(s^{th})$ sector, respectively, and N_0 is the noise spectral density. Thus, the data rate of k^{th} UE over n^{th} subchannel in s^{th} sector being served by the b^{th} beam is $r^s_{k,n} = (B/N_c)\log_2(1 + \Gamma^s_{k,n})$.

C. RF chain power consumption

The power consumption values and quantities of all the components in a RF front-end are listed in Table I [20]. Since power consumption of passive phase-shifter is negligible, the total power consumption per RF chain is expressed as

$$P_{rf} = 2P_{dac} + 2P_m + 2P_{lpf} + P_{lo} + P_{pa} \quad (9)$$

where P_{pa} is a function of P_T and P_{DAC} depends on the sampling frequency F_s and the number of bits b_t as

$$P_{dac} = 1.5 \times 10^{-5} \cdot 2^{b_t} + 9 \times 10^{-12} \cdot b_t \cdot F_s. \quad (10)$$

TABLE I
POWER CONSUMPTION OF COMPONENTS IN A RF CHAIN.

Component	Notation	Power consumption	Quantity
DAC	P_{dac}	Given by (10)	1 per I/Q channel
Low-pass filter	P_{lpf}	14 mW	1 per I/Q channel
Mixer	P_m	0.3 mW	1 per I/Q channel
Phase-shifter	P_{ps}	≈ 0 mW	N_t
Local oscillator	P_{lo}	22.5 mW	1
Power amplifiers	P_{pa}	$P_T/\eta_{pa}, \eta_{pa} = 27\%$	1

An eNB employing N_{RF} number of RF chains will have a single local oscillator shared among all the chains. Therefore, total power consumption of RF front-end at eNB is

$$P_{nrf}(N_{RF}, P_T) = 2N_{RF}(P_{dac} + P_m + P_{lpf} + P_T/(2\eta_{pa})) + P_{lo}. \quad (11)$$

Remark 1: Power amplifier in each RF chain is the main power hungry component of a RF chain and the amount of energy it consumes is a linear function of the transmitted power P_T. Therefore, as given by (6), decreasing the HPBW of the beam will decrease the transmit power requirement, and thereby decreasing the resulting power wastage.

III. JOINT ESTIMATION OF NUMBER OF CONCURRENT BEAMS AND SECTORIZATION SCHEME

We now aim to estimate the optimal number of concurrent beams N^*_{RF} and optimal sectorization scheme S^* required for average long-run UE rate maximization for a given eNB power budget, P_{budget}. We define the long-run UE rate as the total bits received by a UE over one complete cell sweep duration T_{tot}. Therefore, the long-run rate of k^{th} UE in s^{th} sector is

$R_k = T \cdot \sum_{n=1}^{N_c} \pi_{k,n}^s r_{k,n}^s / T_{tot}$, where $T = T_{tot}/\lceil S/N_{RF} \rceil$ and $\pi_{k,n}^s$ is the subchannel assignment variable in OFDM symbol. $\pi_{k,n}^s = 1$ denotes the assignment of n^{th} subchannel to k^{th} UE in s^{th} sector. Also, we define the average long-run UE rate $\bar{R}$ as the average of long-run rate of all UEs given as

$$\bar{R} = \frac{\sum_{j=1}^{U} R_j}{U} = \frac{T}{UT_{tot}} \sum_{s=1}^{S} \sum_{k=1}^{K(s)} \sum_{n=1}^{N_c} \pi_{k,n}^s r_{k,n}^s. \tag{12}$$

In hybrid beamforming the total power consumption at eNB includes total power dissipated predominantly in RF hardware circuitry and power consumed in the transmission of bits. It may be the case that S might not be an integer multiple of N_{RF}. In that case, we assume that during some epochs, in a cell sweep, less than N_{RF} concurrent beams are active since the rest of the sectors have already been scheduled once in the ongoing cell sweep cycle. However, the peak power consumption is constrained by P_{budget} and is given as:

$$P_{peak} = \sum_{s \in \{s_A\}} \sum_{k=1}^{K(s)} \sum_{n=1}^{N_c} P_{k,n}^s + P_{nrf}(N_{RF}, P_T) \tag{13}$$

where $P_{nrf}(\cdot)$ is given by (11) and $\{s_A\}$ denotes the set of sectors concurrently served by all the N_{RF} beams in an epoch.

From (8) we observe that increasing N_{RF}, on one hand, will increase side-lobes interference, thereby decreasing the peak data rate of UE in an epoch, while on the other hand, it will increase T. Thus, we need to choose a suitable value of N_{RF} that maximizes the average long-run UE rate. Moreover, selection of sectorization scheme S will also influence side-lobes interference level and epoch duration T. Further (13) depicts that power is also a function of N_{RF} and S (since P_T is a function of S). Therefore, the optimization problem to estimate S^* and N_{RF}^* that achieves highest $\bar{R}$ for a fixed P_{budget} is formulated as

$$\begin{aligned}
(\mathcal{P}1): &\max_{\pi_{k,n}^s, P_{k,n}^s, S, N_{RF}} \bar{R}(\pi_{k,n}^s, P_{k,n}^s, S, N_{RF}) \\
&\text{s.t. } C11: \sum_{k=1}^{K(s)} \pi_{k,n}^s \leq 1, \forall n, s;\ C12: \pi_{k,n}^s \in \{0,1), \forall k, n, s \\
&\quad C13: \sum_{n=1}^{N_c} \sum_{k=1}^{K(s)} P_{k,n}^s \leq P_T \forall s;\ C14: S \in \mathcal{S} \\
&\quad C15: S \geq N_{RF};\ C16: 0 \leq P_{peak} \leq P_{budget}.
\end{aligned} \tag{14}$$

Constraint $C15$ has a straightforward implication that the total number of beams cannot exceed the total number of sectors in the cell. $\mathcal{P}1$ is jointly non-convex in $(\pi_{k,n}^s, P_{k,n}^s, S, N_{RF})$ and is a NP-hard problem. However, $\mathcal{P}1$ is convex in $\pi_{k,n}^s$ for a fixed value of $P_{k,n}^s$, S and N_{RF}. Therefore, we solve $\mathcal{P}1$ using the following steps:

(i) We decouple the optimal resource allocation of UEs in all of the sectors and optimal (S^*, N_{RF}^*) search. Accordingly, for some combination of (S, N_{RF}) we find the corresponding transmit power P_T given by (6).

(ii) Next, for the resource allocation step in an epoch, initially we assume zero interference power per subchannel in each of the active sectors (concurrently served by N_{RF} beams) and find the corresponding resource allocation for the UEs in all the active sectors independently.

(iii) To achieve a trade-off between system throughput and UE fairness within a sector, we use proportional fairness (PF) subchannel allocation scheme. For analytical simplicity, we begin with the assumption of $P_{k,n}^s = P_T/N_c$ and find $r_{k,n}^s\ \forall k, n$. Therefore, the optimization problem for subchannel allocation in s^{th} active sector in an epoch is formulated as follows:

$$\begin{aligned}
(\mathcal{P}2): &\max_{\pi_{k,n}^s} \sum_{k=1}^{K(s)} \ln \left(\sum_{n=1}^{N_c} \pi_{k,n}^s r_{k,n}^s \right) \\
&\text{s.t. } C21: \sum_{k=1}^{K(s)} \pi_{k,n}^s \leq 1, \forall n;\ C22: \pi_{k,n}^s \in \{0,1\}, \forall k, n.
\end{aligned} \tag{15}$$

We relax $\pi_{k,n}^s$ to be a real number within the interval $[0, 1]$. Then, the Lagrangian formulation of $\mathcal{P}2$ is:

$$\begin{aligned}
\mathcal{L}(\pi_{k,n}^s, \lambda) = &\sum_{k=1}^{N_c} \ln \left(\sum_{n=1}^{N_c} \pi_{k,n}^s r_{k,n}^s \right) \\
&- \sum_{n=1}^{N_c} \lambda_n \left(\sum_{k=1}^{K(s)} \pi_{k,n}^s - 1 \right)
\end{aligned} \tag{16}$$

where $\lambda = [\lambda_1, \ldots, \lambda_n]$ is the non-negative Lagrangian multiplier. Next, we apply KKT condition as:

$$\frac{\partial \mathcal{L}(\pi_{k,n}^s, \lambda)}{\partial \pi_{k,n}^s} = \frac{r_{k,n}^s}{\sum_{n=1}^{N_c} \pi_{k,n}^s r_{k,n}^s} - \lambda_n \leq 0 \tag{17}$$

In (17), if n^{th} subchannel is not allocated of k^{th} UE then $\pi_{k,n}^s = 0, r_{k,n}^s = 0$, and $r_{k,n}^s / \sum_{n=1}^{N_c} \pi_{k,n}^s r_{k,n}^s - \lambda_n \leq 0$. On the other hand, if the n^{th} subchannel is allocated to k^{th} UE then $\pi_{k,n}^s = 1, r_{k,n}^s \neq 0$, and $r_{k,n}^s / \sum_{n=1}^{N_c} \pi_{k,n}^s r_{k,n}^s - \lambda_n = 0$.
This implies that subchannel n is allocated to k^{th} UE by the following rule: $k^* = \underset{k}{\text{argmax}}\ r_{k,n}^s / \sum_{n=1}^{N_c} \pi_{k,n}^s r_{k,n}^s$.

(iv) Having found $\pi_{k,n}^s\ \forall k, n$ from step (iii), we allocate a fraction of total power, $P_T|\Omega_k|/N_c$, to each UE, where $\Omega_k = \sum_{n=1}^{N_c} \pi_{k,n}^s$. Thereafter, we perform power allocation individually for each UE using water-filling over its allocated subchannels.
Note: We follow this sub-optimal resource allocation procedure because estimation of (S^*, N_{RF}^*) is a relative search over all $\bar{R}\ \forall S \in \mathcal{S}$.

(v) Solving for sub-optimal resource allocation in one beam will influence the resource allocation of UEs in other active sectors, since the subchannels experience side-lobes interference from the concurrent beams. Hence, steps (iii)–(iv) are repeated to find the best resource allocation strategy of all the concurrently active sectors so that the peak cell sum rate in the current epoch is maximized.

(vi) Steps (ii)–(v) are carried out for all the epochs in a cell sweep cycle to calculate $\bar{R}$ using (12).

(vii) The above steps are repeated for all possible combinations of (S, N_{RF}) while satisfying $C14, C15$ and $C16$ to find the optimal (S^*, N^*_{RF}) that achieves maximum $\bar{R}$.

IV. Complexity Analysis

1) Subchannel allocation: For a system with $K(s)$ UEs and N_c subchannels in a sector, the PF resource allocation using the steps (i)–(iv) has a complexity of $\mathcal{O}(N_c \sum_{k=1}^{K(s)} |\Omega_k| \log(|\Omega_k|))$. The final complexity of instantaneous rate convergence is $\mathcal{O}(\zeta N_c \sum_{k=1}^{K(s)} |\Omega_k| \log(|\Omega_k|))$ where ζ is the number of iterations required at step (v).

2) Joint S^* and N^*_{RF} estimation: Step (vii) is solved to jointly estimate S^* and N^*_{RF} that maximizes $\bar{R}$ for a given eNB power budget. In the worst case, it performs comparison over all the combinations of S and N_{RF}. Hence, the overall worst-case complexity of $\mathcal{P}1$ is $\mathcal{O}(\zeta N_c |\mathcal{S}|^2 \sum_{k=1}^{K(s)} |\Omega_k| \log(|\Omega_k|))$.

V. Results and Discussions

In this section, we present the numerical simulation results generated using MATLAB. The simulation set-up configurations are given in Table II.

Fig. 2(a) shows the EIRP beam pattern corresponding to different number of antenna elements connected to single RF unit. Also, it can be observed that the peak EIRP value is static irrespective of transmit beam gain and hence, a constant cell range is ensured in the simulations. It is notable that the interfering EIRP level in side-lobes diminishes with decreasing beamwidth. Fig. 2(b) shows the convergence of peak sector sum rate of step (v). Here, the second maximum peak sector sum rate in a epoch occurs in less than 30 iterations and the first peak is not accounted for due to the initial assumption of zero interference power per subchannel (step (ii)). Also, due to no interference assumption at 1^{st} iteration, the sum rate of a sector is same irrespective of number of beams employed. From Fig. 2(b) we also observe that the peak sector throughput degrades on increasing N_{RF} since the angular separation between the beams reduces thereby increasing the side-lobe interference experienced by the UEs in a sector.

TABLE II
Simulation Parameters and Values

Parameter	Interpretation	Value
D	Cell Diameter	400 m
f_c	Carrier frequency	28 GHz
B	Bandwidth	1 GHz
EIRP	Effective isotropic radiated power	52 dBm [19]
U	Number of UEs	400
N_c	Number of subchannels	32
θ	HPBW	1^o to 25^o
N_t	Antenna elements per RF unit	5 to 115
d'	Inter-element ULA spacing	$\lambda_c/2$
S	Number of sectors	$\lceil 360/\theta \rceil$
N_{RF}	Number of concurrent beams	$\leq S$
N_0	Noise spectral density	-174 dBm/Hz
L_k	Number of MPCs	4
$\alpha_{k,l}$	l^{th} MPC fading parameter	Rician (LOS), Rayleigh (NLOS)
K_R	Rician fading parameter	8 dB

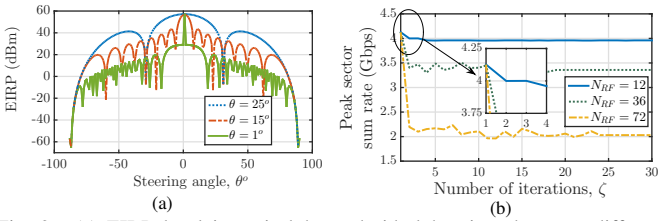

Fig. 2. (a) EIRP level in main-lobe and side-lobes in a beam at different beamwidth. (b) Convergence of peak sector sum rate in an epoch for $U = 400$ and $S = 72$.

However, Fig. 3 shows that despite a decrease in peak throughput per sector, the average long-run UE rate $\bar{R}$ improves with increasing N_{RF} for a constant S. The improvement in $\bar{R}$ with N_{RF} can be attributed to the increase in T from using a large number of concurrent beams that overcomes the rate loss due to increased interference level. Also, we observe from Fig. 3 and Fig. 4 that, for a fixed value of N_{RF}, using the narrowest beam is not always beneficial even though narrow beams offer reduced inter-beam interference. This is because a narrower beam (or a larger value of S) means a shorter sector sojourn time, resulting in a lower $\bar{R}$.

Fig. 5 depicts that P_{peak} (sum of total power transmitted and consumed in RF hardware) rises with increasing N_{RF} and falls with S, as explained in Remark 1. The value of N_{RF} is thus limited by P_{budget}. For example, for $U = 400$, $(S^*, N^*_{RF}) = (72, 72)$ is the optimal solution with highest $\bar{R}$ when there is no power budget constraint at eNB with maximum achievable $\bar{R} = 458.72$ Mbps, and $P_{peak} = 271.63$ W. However, for a given $P_{budget} = 50$ W the optimum solution is $(S^*, N^*_{RF}) = (30, 15)$ with $\bar{R} = 210.58$ Mbps and $P_{peak} = 49.07$ W.

In Fig. 6 we compare the $\bar{R}$ achieved using the proposed system model and the models in [12], [13]. Both [12], [13] use a fully-connected hybrid structure that serves maximum N_{RF} UEs in an epoch by dedicating one RF unit per scheduled UE. For the sake of fair comparison, we fix the total number of antenna elements at eNB equal to 256 and set keep $N_t \leq 256/N_{RF}$ in the proposed model. Since utmost N_{RF} UEs can be scheduled in an epoch using schemes in [12], [13] so, we fix T_{tot} and divide it equally over the number of epochs

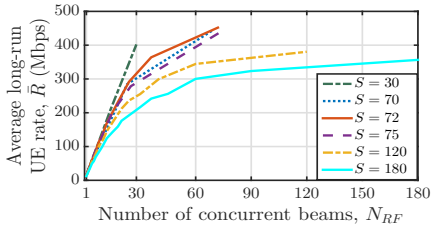

Fig. 3. Illustration of $\bar{R}$ as a function of N_{RF} for different S and $U = 400$.

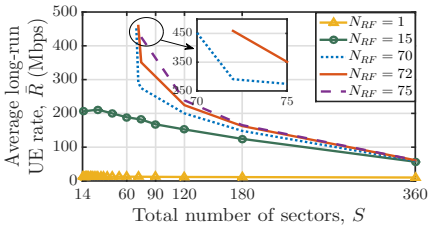

Fig. 4. Illustration of $\bar{R}$ as a function of S for different N_{RF} and $U = 400$.

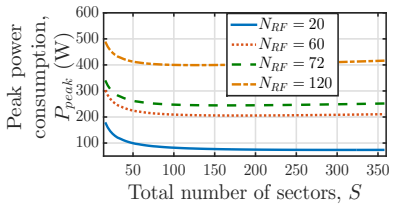

Fig. 5. Illustration of P_{peak} as a function of S and N_{RF}.

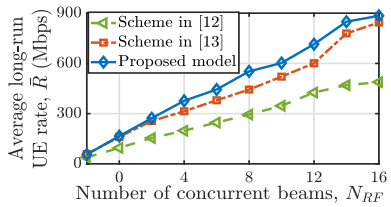

Fig. 6. Comparison of achievable $\bar{R}$ with different schemes.

required to serve all UEs. For computational convenience here we take $U = 100$. Further, Table III compares the scheduling complexity of the proposed model over some of the existing competitive UE scheduling schemes, as a function of U, N_{RF} and N_t at eNB. In our proposed model all the UEs that are located within the beam coverage area are grouped and served simultaneously, as mentioned in I-B. Hence, scheduling is independent of U and number of groups is equal to N_{RF}. Therefore, comparable performance can be achieved with reduced computation complexity using proposed approach.

TABLE III
UE SCHEDULING COMPLEXITY

Scheduling Method	**Complexity**
Based on SVD decomposition [21]	$\mathcal{O}(N_{RF}^2 N_t)$
Based on channel's second order characteristics and greedy algorithm [12]	$\mathcal{O}(U)$
Based on AoD's similarities [13]	$\mathcal{O}(UN_{RF}\eta_I)$, here η_I is number of iterations to converge
Proposed method	$\mathcal{O}(N_{RF})$

VI. Conclusion

In this paper we have investigated the sub-array hybrid beamforming structure for outdoor mmWave scenario. For a system having fewer RF units at the eNB compared to the UE population we have proposed a reduced complexity system model to serve multiple UEs per beam at a time over wideband mmWave channel. From simulations we have observed that though interference from the side-lobes of concurrent beams reduces the peak sector throughput, the time-averaged data rate of UEs improves. Also, it has been shown that using the narrowest beamwidth is not optimal. From the point of view of power requirements, it has been studied that having higher number of RF units amplifies the eNB power budget significantly. However, the total power required at the eNB is a function of beam HPBW as well. Therefore, the power budget plays a crucial role in deciding the optimum number of concurrent beams and corresponding sector beamwidth.

VII. Acknowledgement

This work has been supported by the DST under Grant INT/Korea/P-46 and the DoT under Grant 4-23/5G-test-bed/2017-NT.

References

[1] A. L. Swindlehurst, E. Ayanoglu, P. Heydari, and F. Capolino, "Millimeter-wave massive MIMO: The next wireless revolution?" *IEEE Commun. Mag.*, vol. 52, no. 9, pp. 56–62, 2014.

[2] H. Shokri-Ghadikolaei and C. Fischione, "The transitional behavior of interference in millimeter wave networks and its impact on medium access control," *IEEE Trans. Commun.*, vol. 64, no. 2, pp. 723–740, 2015.

[3] I. Ahmed, H. Khammari, A. Shahid, A. Musa, K. S. Kim, E. De Poorter, and I. Moerman, "A survey on hybrid beamforming techniques in 5G: Architecture and system model perspectives," *IEEE Commun. Surveys Tuts.*, vol. 20, no. 4, pp. 3060–3097, 2018.

[4] S. Kumar, S. Suman, and S. De, "Dynamic resource allocation in UAV-enabled mmWave communication networks," *IEEE Internet of Things J.*, vol. 8, no. 12, pp. 9920–9933, 2021.

[5] F. Sohrabi and W. Yu, "Hybrid analog and digital beamforming for mmWave OFDM large-scale antenna arrays," *IEEE J. Sel. Areas Commun.*, vol. 35, no. 7, pp. 1432–1443, 2017.

[6] B. Wang, M. Jian, F. Gao, G. Y. Li, and H. Lin, "Beam squint and channel estimation for wideband mmWave massive MIMO-OFDM systems," *IEEE Trans. Sig. Process.*, vol. 67, no. 23, pp. 5893–5908, 2019.

[7] L. Qianrui, "Hybrid precoding for wideband multi-user MIMO millimeter wave system," in *IEEE Wireless Commun. Net. Conf. (WCNC)*, 2019.

[8] T. Mir, M. Z. Siddiqi, U. Mir, R. Mackenzie, and M. Hao, "Machine learning inspired hybrid precoding for wideband millimeter-wave massive mimo systems," *IEEE Access*, vol. 7, pp. 62 852–62 864, 2019.

[9] C.-E. Chen, "An iterative hybrid transceiver design algorithm for millimeter wave MIMO systems," *IEEE Wireless Commun. Letters*, vol. 4, no. 3, pp. 285–288, 2015.

[10] W. Ni and X. Dong, "Hybrid block diagonalization for massive multiuser MIMO systems," *IEEE Trans. Commun.*, vol. 64, no. 1, pp. 201–211, 2015.

[11] C. A. Viteri-Mera, F. L. Teixeira, and K. Sainath, "Interference-nulling time-reversal beamforming for mm-Wave massive MIMO systems," in *IEEE Int. Conf. Microwaves, Commun., Antennas and Electronic Systems (COMCAS)*, 2015, pp. 1–5.

[12] A. Adhikary, E. Al Safadi, M. K. Samimi, R. Wang, G. Caire, T. S. Rappaport, and A. F. Molisch, "Joint spatial division and multiplexing for mm-wave channels," *IEEE J. Sel. Areas Commun.*, vol. 32, no. 6, pp. 1239–1255, 2014.

[13] A. Masmoudi and T. Le-Ngoc, "User grouping and hybrid RF/baseband precoding for multi-user massive MIMO systems," *IEEE Trans. Veh. Technol.*, 2020, http://doi:0.1109/TVT.2020.3009138.

[14] N. Varshney and S. De, "Optimum downlink beamwidth estimation in mmWave communications," *IEEE Trans. Commun.*, vol. 69, no. 1, pp. 544–557, 2021.

[15] T. S. Rappaport, Y. Xing, G. R. MacCartney, A. F. Molisch, E. Mellios, and J. Zhang, "Overview of millimeter wave communications for fifth-generation (5G) wireless networks—With a focus on propagation models," *IEEE Trans. Antennas and Propagation*, vol. 65, no. 12, pp. 6213–6230, 2017.

[16] M. R. Akdeniz, Y. Liu, M. K. Samimi, S. Sun, S. Rangan, T. S. Rappaport, and E. Erkip, "Millimeter wave channel modeling and cellular capacity evaluation," *IEEE J. Sel. Areas Commun.*, vol. 32, no. 6, pp. 1164–1179, 2014.

[17] O. El Ayach, S. Rajagopal, S. Abu-Surra, Z. Pi, and R. W. Heath, "Spatially sparse precoding in millimeter wave MIMO systems," *IEEE Trans. Wireless Commun.*, vol. 13, no. 3, pp. 1499–1513, 2014.

[18] C. A. Balanis, *Antenna theory: analysis and design*. John wiley & sons, 1997.

[19] FCC. (2015) *Notice of Proposed Rulemaking*. FCC-15-138A1.

[20] L. N. Ribeiro, S. Schwarz, M. Rupp, and A. L. de Almeida, "Energy efficiency of mmWave massive MIMO precoding with low-resolution DACs," *IEEE J. Sel. Topics Sig. Process.*, vol. 12, no. 2, pp. 298–312, 2018.

[21] P. Zhao and Z. Wang, "Joint user scheduling and hybrid precoding for multi-user mmWave systems with two-layer PS network," in *IEEE Global Commun. Conf. (GLOBECOM)*, 2018, pp. 1–6.